Decoration of Zinc Oxide Nanoparticles with Aluminum Nanoparticles by Explosive Strips Method

Mena L. Badran
Saba. J. Kadhem

Department of Physics, College of Science, University of Baghdad, Baghdad, IRAQ

In this study, aluminum nanoparticles (Al NPs) were prepared using explosive strips method in double-distilled deionized water (DDDW), where the effect of five different currents (25, 50, 75, 100 and 125 A) on particle size and distribution was studied. Also, the explosive strips method was used to decorate zinc oxide particles with Al particles, where Al particles were prepared in suspended from zinc oxide with DDDW. Transmission electron microscopy (TEM), UV-visible absorption spectroscopy, and x-ray diffraction are used to characterize the nanoparticles. XRD pattern were examined for three samples of aluminum particles and DDDW prepared with three current values (25, 75 and 125 A) and three samples prepared with the same currents for zinc oxide suspension with aluminum particles and DDDW. It was observed that when increasing the percentage of prepared Al particles in the suspension consisting of zinc oxide and DDDW, the energy gap of zinc oxide gradually decreased in the samples. Transmission electron microscopy (TEM) analysis is conducted to examine the size, shape, and aggregation of the nanoparticles. The TEM images reveal that the Al nanoparticles exhibit a quasi-spherical shape. The particle size distribution analysis shows that the average crystal size of Al decreases with an increase in the detonation current. This method yields particle with average sizes within the range of 20 to 90 nm. When decorating zinc oxide particles by generating Al nanoparticles inside a suspension of zinc oxide and DDDW, the size of the resulting particles increases with increasing current.

Keywords: Explosive strips method; Nanoparticles; Atomic force microscopy; Optical properties
Received: 01 September 2023; **Revised:** 25 September 2023; **Accepted:** 02 October 2023

1. Introduction

In recent years, nanoscience and nanotechnology have revolutionized various fields by offering unprecedented opportunities for designing and engineering advanced materials with tailored properties [1-3]. There have been numerous reports of physical and chemical processes for producing nanoparticles, one of which is the use of plasma (exploding wire method) [4-8]. Among the wide range of nanomaterials, metal oxide nanoparticles (NPs) have gained significant attention due to their unique physical and chemical characteristics [9-12]. Zinc oxide (ZnO) NPs, in particular, have demonstrated remarkable properties, including high surface area, photocatalytic activity, and antimicrobial efficacy, making them suitable for diverse applications such as optoelectronics, sensors, and environmental remediation [13-15]. It is a semiconductor with a wide bandgap and a direct band gap width of 3.37 eV [16-19]. Despite their inherent advantages, the performance and functionality of ZnO NPs can be further improved by incorporating other functional materials. In this context, aluminum (Al) NPs have emerged as a promising candidate due to their excellent thermal stability, electrical conductivity, and corrosion resistance [20-21]. The traditional methods for synthesizing composite nanomaterials involve complex and time-consuming procedures, often accompanied by challenges such as poor homogeneity and limited control over the size, shape, and distribution of the NPs [22]. To overcome these limitations, a novel approach called the explosive strips method has recently been proposed, which enables the decoration of ZnO NPs with Al NPs in a facile and efficient manner [23]. This method involves the controlled explosion of Al strips in close proximity to ZnO NPs, leading to the deposition of Al NPs onto the surface of ZnO NPs [24]. The novelty of this research lies in the fact that the research presents the preparation of composite nanoparticles using explosive strips. The utilization of this method for the synthesis of composite nanoparticles is a novel approach that offers advantages such as simplicity, efficiency, and control over particle size and distribution [25]. Furthermore, the optical enhancement of ZnO nanoparticles through the incorporation of aluminum nanoparticles offers the advantage of controllable energy gap modulation, expanding their potential applications. The study demonstrates that the energy gap gradually decreases with an increase in the proportion of aluminum nanoparticles, indicating modifications in the electronic properties of the composite material [26]. This finding enhances the understanding of the electronic interactions and band structure modifications in composite nanoparticles. The

decorated ZnO-Al NPs are expected to exhibit enhanced conductivity, improved catalytic performance, and increased stability, enabling their utilization in various technological applications [27-28].

We describe the characterization and unusual optical properties of Al and Al-ZnO nanoparticles prepared from the Al alloy using the exploding strip method in the current study. X-ray diffraction (XRD), UV-visible, and scanning electron microscopy have all been used in the physical-chemical description (TEM). Also, optical emission spectroscopy was used to investigate the properties of the plasma produced by the electric explosion wire method (EEW) [29-30].

2. Experimental Part

Figure (1) shows the equipment needed to prepare metallic nanoparticles from a liquid media explosive strip system. The system consists of two electrodes, the negative electrode is an Al strip with a length of 25 cm and a thickness of 0.1 mm, and the positive electrode is an Al sheet with dimensions of (4.5×3.5) cm and a thickness of 0.15 mm. The strip and the board are made of the same material, but with reverse polarity. The electrodes were placed in a Pyrex beaker containing 100 ml of deionized double-distilled water (DDDW).

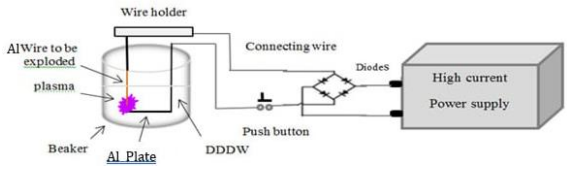

Fig. (1) Exploding strip system

High electric currents (with values of 25, 50, 75, 100 and 125 A) were passed through the Al tape. The strip and hot plate vaporize into plasma upon contact. The aluminum strip is contacted the aluminum slide approximately 40 times for each value of the passing current. X-ray is used to determine the crystallographic structure of materials. In the wavelength range of 180–880 nm, ultraviolet-visible light from a dual-beam spectrophotometer was used to examine the absorption spectrum. Utilizing TEM, the particle size and particle size distribution were determined. Changes in the absorption spectrum over time were studied to evaluate the stability of the prepared nanoparticles.

3. Results and discussion

The UV-visible analysis was conducted immediately following the determination of the chemical composition of Al nanoparticles and Al particles in the presence of zinc oxide. The UV-vis spectrum, as depicted in Fig. (2), was acquired using absorption mode within the range of 180 to 880 nm. Figures (2a and b) vividly demonstrate changes in the absorption spectrum, depicting how absorbance varies with wavelength for five different current values utilized in nanoparticle preparation. The rise in absorbance with increasing passing current is indicative of the heightened power input into the system.

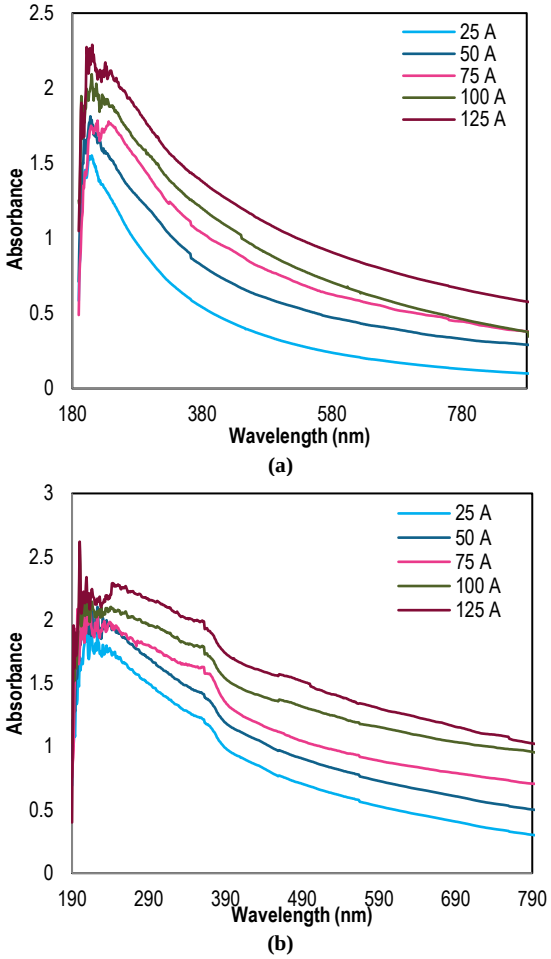

Fig. (2) UV-visible Al spectra generated by EEW in DDDW at various currents: (a) Al and (b) Al-ZnO

The correlation between detonation current and absorbance in UV-Vis spectroscopy can be attributed to several factors. An increase in detonation current leads to a higher yield of prepared nanoparticles, consequently elevating the total particle surface area and augmenting energy absorption. Additionally, the explosive strip method is capable of producing nanoparticles with diverse surface roughness and morphology. With heightened detonation current, the energy released during the explosion induces more substantial fragmentation and vaporization of the strip material. This, in turn, yields nanoparticles with coarser surfaces, non-uniform shapes, or amplified surface area-to-volume ratios. These factors collectively amplify interactions between light and matter, resulting in an amplified absorbance in the UV-Vis range, aligning with findings in [24]. Employing this correlation, the energy gap can be computed based on direct transitions [31-35].

$$(\alpha h\nu)^2 = A(h\nu - E_g) \quad (1)$$

where A represents a constant, E_g represents an energy gap, and *hv* represents the energy of a photon. The symbol α denotes the absorption coefficient (α), which can be derived from transmittance by (-ln1/T)/d as T is the transmittance and d is the film thickness. $(\alpha hv)^2$ and *hv* were used to plot their respective relationship curves. The energy gap for permitted direct transmission of the ZnO films in the presence of aluminum ranged from 2.55 to 3.12 eV, as illustrated in Fig. (3).

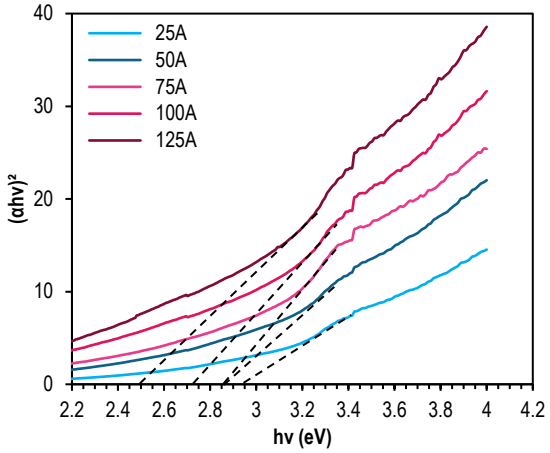

Fig. (3) The relationship between $(\alpha hv)^2$ and hv for Al-ZnO

When Al is introduced into a different material, it acts as a patterning material, introducing patterned states into the band gap. This in turn affects the energy levels and conductivity of the host material. In the present case, nanoparticles act as decoration on the ZnO surface, leading to modifications in energy levels and reduction of the band gap. Furthermore, when compared to bulk materials, nanoparticles have a substantially higher surface-to-volume ratio. This augmented surface area allows for enhanced interaction with the surrounding medium, in this instance, water molecules. These interactions can facilitate charge transfer and give rise to the formation of interfacial states, consequently influencing the electronic properties of the composite material. The presence of Al nanoparticles on the surface of ZnO has the capacity to alter the band structure, ultimately resulting in a diminished energy gap for ZnO gradually in the samples. It is evident that with escalating currents, the energy gap diminishes proportionally to the increase in Al content within the sample, corroborating findings in [26] as presented in table (1).

Table (1) The energy gap for Al-ZnO

Current(Am)	25	50	75	100	125
E_g (eV)	3.12	2.79	2.68	2.59	2.55

Figure (4) depicts the diffraction peaks of Al nanoparticles prepared using the explosive strip method at three distinct currents (25, 75, and 125 A). The XRD pattern was captured within a 2θ angle range spanning from 30° to 80°, as exemplified in Figure 4. peaks are observed at 38.17°, 44.4°, 64.9°, and 78.37°, corresponding to reflects from the (111), (200), (220), and (311) planes, respectively. This indicates a face-centered cubic structure according to standard card in (JCPDS card No. 00-004-0787), and this agrees with [36]. For the determination of the average crystallite size, Scherrer's formula, outlined in references [37-42], is employed, as follows:

$$D = \frac{0.9\,\lambda}{\beta COS\,\theta_\beta} \qquad (2)$$

where λ represents the wavelength of the x-ray and β signifies the maximum of the Bragg diffraction peak or the Full Width at Half Maximum (FWHM) of the XRD peak measured in radians. The average crystallite size for Al at the three currents (25, 75, and 125 A) was determined as follows: 28.721 nm, 20.832 nm, and 18.653 nm, respectively.

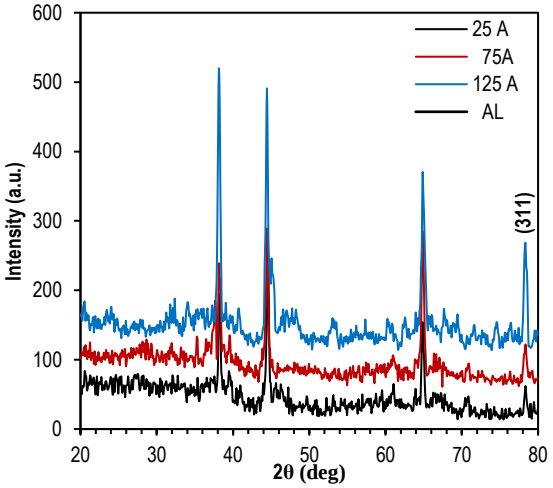

Fig. (4) XRD patterns of Al at different currents

Figure (5) illustrates the diffraction peaks of (Al-ZnO) nanoparticles prepared by the explosive strips at three different currents (25, 75, and 125 A). The XRD pattern was recorded with angles of 2θ ranging from 30° to 80°, as shown in Figure (5). Peaks were observed at 38.17°, 44.4°, 64.9°, and 78.37°, which are related to Al corresponding to reflects from (111), (200), (220), and (311), respectively. These results align well with the normative values for the data presented (JCPDS card No. 00-004-0787). The average crystallite size of Al at three currents (25, 75, and 125 A) was calculated as follows: 67.1 nm, 73.9 nm, and 82.7 nm, respectively.

The diffraction peaks for $ZnAl_2O_4$ were observed at 2θ positions of 59.2°, 74.28°, and 77.57°, indicating reflects from (511), (620), and (533), respectively. Which shows matching with the (JCPDS card no. 00-005-0669), and agrees with diffraction peaks in above mentioned [43]. The average crystallite size of $ZnAl_2O_4$ at the three currents (25, 75, and 125 A) was calculated as follows: 58.5 nm, 65.9 nm, and 80.9 nm, respectively. Additionally, diffraction peaks for ZnO were observed at 2θ positions 31.8°, 34.4°, 36.3°, 47.5°, 56.6°, 62.8°, 66.4°, 67.9°, 69.1°, 72.5°, and 76.9° are

found to be relative to (100), (002), (101), (102), (110), (103), (200), (112), (201), (004), and (202) planes. These results are generally consistent with the normative values for the data presented on JCPDS card No. (79-2205), substantiating that ZnO possesses a crystalline hexagonal structure, this agrees with [44]. The average crystallite size of ZnO at the three currents (25, 75, and 125A) was calculated as follows: 56 nm, 57.9 nm, and 69.3 nm, respectively.

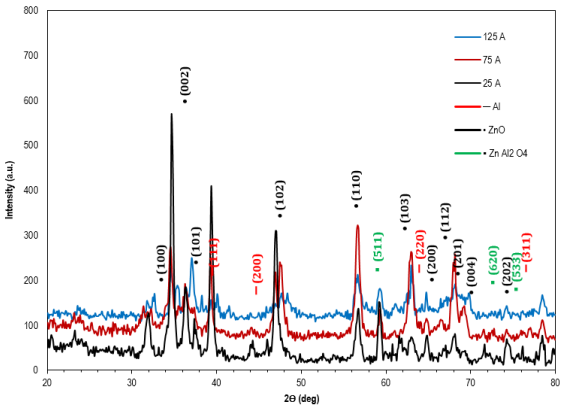

Fig. (5) XRD patterns of Al-ZnO at different currents

Figures (4) and (5) reveal that with an increase in the value of the explosive current in the experiment, the diffraction peaks of Al and $ZnAl_2O_4$ increase, while the intensity of the peaks of ZnO decreases [45]. This phenomenon can be attributed to the formation of the $ZnAl_2O_4$ compound during the process of sintering ZnO particles with Al nanoparticles via the explosive strip method. This results from the prepared of highly reactive Al nanoparticles, possessing both high surface area and reactivity. When they come into contact with ZnO particles during the sintering process, redox reactions occur, wherein Al nanoparticles undergo oxidation reactions in the presence of oxygen. This leads to the formation of an Al oxide layer on the surface of Al, which then reacts with ZnO particles to produce the compound $ZnAl_2O_4$, commonly known as zinc aluminate. An increase in the current value leads to a rise in the temperature of the electrons and, consequently, an increase in the energy gained from the electron plasma, resulting in a higher number of nanoparticles.

In summary, the increase in current leads to a decrease in the crystallite size of the Al nanoparticles. The X-ray diffraction pattern in Fig. (5) further indicates that the diffraction intensities of ZnO can decrease with increasing detonation current. When ZnO is decorated with Al nanoparticles, the strength of the X-ray diffraction (XRD) peaks of the ZnO decreases, which can be explained by an increase in the dispersion of the Al nanoparticles.

Transmission Electron Microscopy (TEM) analysis is employed to confirm the composition of the nanoparticles and offers insights into their size, shape, and aggregation characteristics. Figure (6) displays TEM images of Al nanoparticles, revealing their quasi-spherical shape, which is in agreement with previous studies [46-49]. For the determination of particle size, TEM image analysis was conducted using ImageJ software. The size distribution graph in Fig. (6) indicates that the average particle size of Al at the three currents (25, 75, and 125 A) was calculated to be 36.2 nm, 26.3 nm, and 20.7 nm, respectively. The detonation current corresponds to the electrical current supplied to the detonation system. With an increase in current, the energy input into the system also rises. This elevated energy input results in a more vigorous and intense detonation process. The higher energy input during detonation leads to a more forceful fragmentation of the Al material.

The shock waves and rapid expansion generated by the detonation process cause the material to disintegrate into smaller particles. The rapid cooling effect, brought about by the expansion and dispersion of detonation products, hinders the agglomeration or coalescence of the newly formed Al nanoparticles. This quenching effect aids in maintaining the smaller particle size and prevents their growth into larger particles. Figure (7) illustrates the ZnO particles decorated with Al nanoparticles. The dark inner part represents the core (ZnO), while the surrounding bright part signifies the shell this agrees with [50]. The core/shell structure fabricated in our work involves a core of zinc oxide (ZnO) particles surrounded by a shell composed of aluminum (Al) nanoparticles. This configuration is achieved through a process in which aluminum nanoparticles, generated during the explosive strip method, adhere to the surface of pre-existing ZnO particles. This adhesion forms a distinctive shell around the ZnO core. The resulting core/shell structure is characterized by the presence of both ZnO and Al, with the aluminum nanoparticles acting as a protective outer layer for the ZnO core. The size distribution graph in Figure (7) reveals that the average particle size of ZnO/Al (core/shell) at the three currents (25, 75, and 125 A) was calculated to be 60.1 nm, 71.8 nm, and 86.9 nm, respectively. It can be deduced from TEM analysis that the particle size increases with an escalating current.

The decoration of ZnO nanoparticles with Al nanoparticles, prepared through the explosive strip method, can be attributed to the generation of high temperatures, pressures, and shock waves. These factors cause the strip to rapidly disintegrate, transforming into Al nanoparticles. These nanoparticles are propelled with significant energy into the surrounding environment. Additionally, during the explosion process, the Al nanoparticles produced are propelled and dispersed in the vicinity. In this scenario, they come into contact with pre-existing ZnO nanoparticles. When the Al nanoparticles collide with the surface of the ZnO

nanoparticles, they may adhere due to various forces, such as van der Waals forces, electrostatic interactions, or chemical bonding, contingent on specific conditions and surface properties.

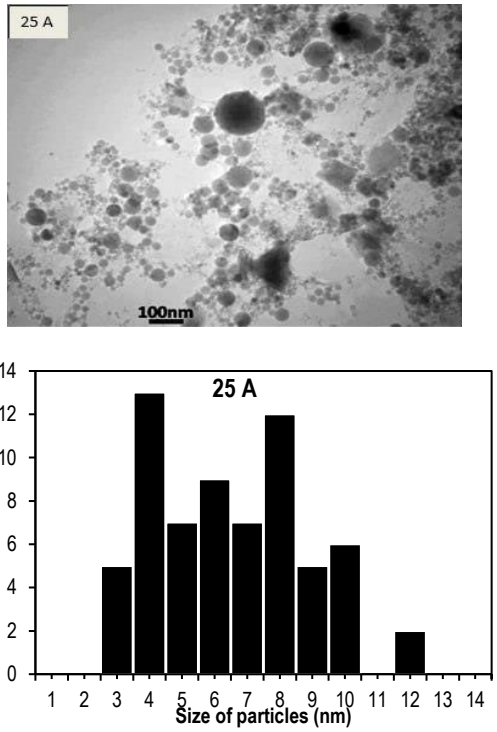

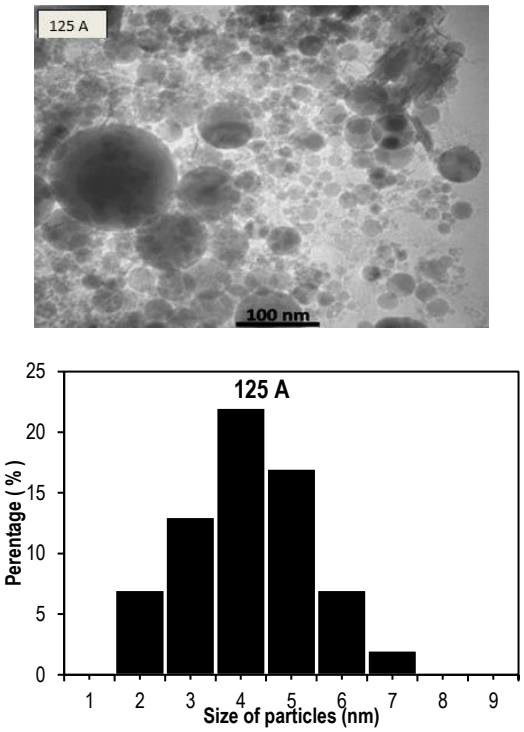

Fig. (6) Shows typical images obtained by transmission electron microscopy (TEM) of Al nanoparticles produced at three different currents (25 A, 75 A, and 125A)

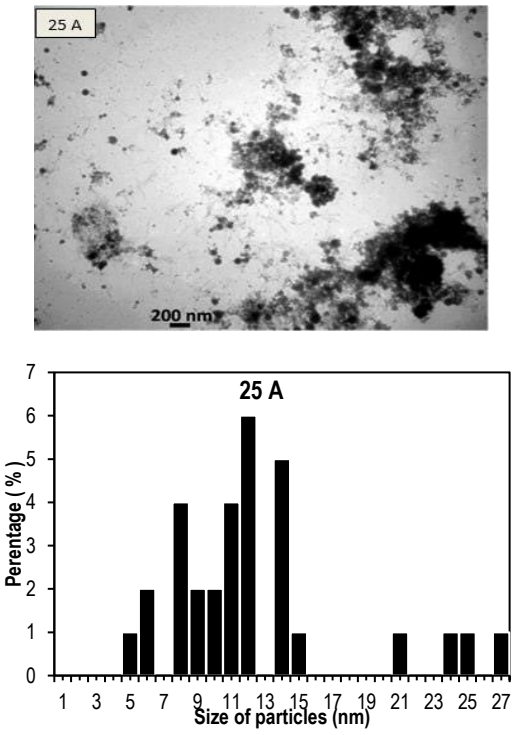

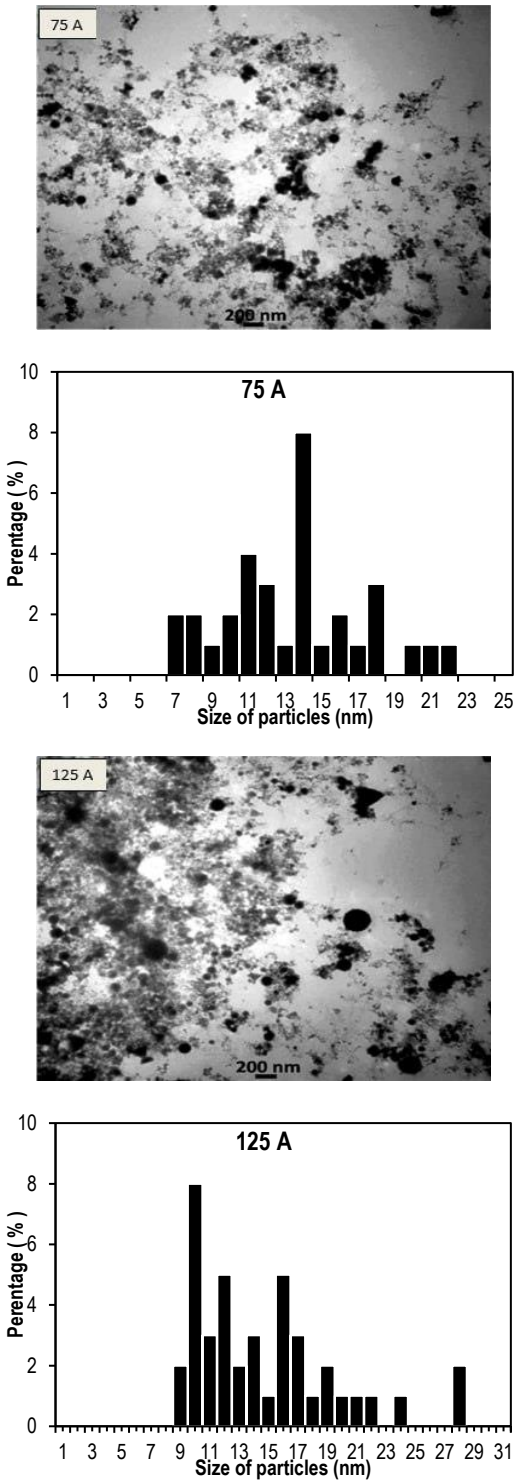

Fig (7) shows typical images obtained by transmission electron microscopy (TEM) of Al-ZnO nanoparticles produced at three different currents (25 A, 75 A, and 125 A)

The combination of the specific characteristics of ZnO and Al nanoparticles, including their sizes, surface chemistry, and reactivity, contributes to the decoration phenomenon. The adhesion of Al nanoparticles onto ZnO nanoparticles results in the formation of composite structures, where the Al nanoparticles are distributed and anchored on the surface of the ZnO nanoparticles.

4. Conclusion

This study presents a concise yet highly efficient method for the synthesis of nanoparticles. All the synthesized nanoparticles showed nanoscale dimensions. DDDW-induced explosive dissociation of aluminium (Al) ribbons in a ZnO suspension. This innovative approach led to the adhesion of ZnO nanoparticles, generating composite structures with Al nanoparticles adhered to the surface of ZnO particles. The absorbance increased proportionally to increasing current, however the energy gap of ZnO dropped as the fraction of Al in the sample increased. The crystalline structures of $ZnAl_2O_4$, ZnO, and aluminum were confirmed by x-ray diffraction.

References

[1] E. Hao, G.C. Schatz and J.T. Hupp, "Synthesis and optical properties of anisotropic metal nanoparticles", *J. Fluoresc.*, 14 (2004) 331-341.

[2] L. LaConte, N. Nitin and G. Bao, "Magnetic nanoparticle probes", *Mater. Today*, 8(5) (2005) 32-38.

[3] N.K. Hussein and S.J. Kadhem, "The optical properties of C\Mg, nano-rods produced by the explosion wire technique", *IOP J. Phys.: Conf. Ser.*, 2114(1) (2021) 12041.

[4] H.R. Humud, "Synthesis of Au–Ag–Cu trimetallic alloy nanoparticles prepared by electrical exploding wire technique in distilled water", *Iraqi J. Phys.*, 16(39) (2018) 81-92.

[5] H.R. Humud, "Optical emission spectroscopy for studying the exploding copper wire plasma parameters in distilled water", *Iraqi J. Phys.*, 15(35) (2018) 142-147.

[6] S.H. Abdullah, "Effect of current intensity on structural properties of cupper iodine nanoparticles produced by exploding Cu wire", *Iraqi J. Phys.*, 17(41) (2019) 1-6.

[7] S.M. Fathi and S.J. Kadhim, "Optical Emission Spectroscopy for Studying Fe Plasma Parameters Produced by Exploding Wire Technique in Carbon Nanotubes - Water Colloid", *Iraqi J. Sci.*, 63(1) (2022) 163-169.

[8] N.K. Hussein and S.J. Kadhem, "Spectroscopic diagnosis of Arc Carbon and Magnesium plasma", *Iraqi J. Sci.*, 63(6) (2022) 2492-2501.

[9] R.S. Mohammed, "Synthesis of CuO/ZnO and MgO/ZnO Core/Shell Nanoparticles with Plasma Jets and Study of their Structural and Optical Properties", *Karbala Int. J. Mod. Sci.*, 8(2) (2022) 213-222.

[10] H. Kumar et al., "Flower-based green synthesis of metallic nanoparticles: Applications beyond fragrance", *Nanomaterials*, 10(4) (2020) 766.

[11] M.S. Chavali and M.P. Nikolova, "Metal oxide nanoparticles and their applications in nanotechnology", *SN Appl. Sci.*, 1(6) (2019) 607.

[12] S. Gautam et al., "Metal oxides and metal

organic frameworks for the photocatalytic degradation: A review", *J. Environ. Chem. Eng.*, 8(3) (2020) 103726.
[13] A. Hatamie et al., "Zinc oxide nanostructure-modified textile and its application to biosensing, photocatalysis, and as antibacterial material", *Langmuir*, 31(39) (2015) 10913-10921.
[14] V.J. Raj et al., "Application of zinc oxide nanoflowers in environmental and biomedical science", *BBA Adv.*, 2 (2022) 100051.
[15] A. Asture et al., "Investigation of properties and applications of ZnO polymer nanocomposites", *Polym. Bull.*, 80(4) (2023) 3507-3545.
[16] S.S. Kumar et al., "Synthesis, characterization and optical properties of zinc oxide nanoparticles", *Int. Nano Lett.*, 3 (2013) 1-6.
[17] M. Suchea et al., "ZnO transparent thin films for gas sensor applications", *Thin Solid Films*, 515(2) (2006) 551-554.
[18] A.H. Ramelan et al., "ZnO wide bandgap semiconductors preparation for optoelectronic devices", *IOP Conf. Ser.: Mater. Sci. Eng.*, 176(1) (2017) 12008.
[19] M.K. Dhahir, "Enhanced Physical Absorption Properties of ZnO Nanorods by Electrostatic Self-Assembly with Reduced Graphene Oxide and Decorated with Silver and Copper Nanoparticles", *Iraqi J. Phys.*, 19(48) (2021) 66-78.
[20] H.R. Ghorbani, "A review of methods for synthesis of Al nanoparticles", *Orient. J. Chem.*, 30(4) (2014) 1941-1949.
[21] N. Kumar and K. Biswas, "Cryomilling: An environment friendly approach of preparation large quantity ultra refined pure aluminium nanoparticles", *J. Mater. Res. Technol.*, 8(1) (2019) 63-74.
[22] A. Bendre et al., "Recent developments in microfluidic technology for synthesis and toxicity-efficiency studies of biomedical nanomaterials", *Mater. Today Adv.*, 13 (2022) 100205.
[23] A.S. Wasfi, H.R. Humud and N.K. Fadhil, "Synthesis of core-shell Fe_3O_4-Au nanoparticles by electrical exploding wire technique combined with laser pulse shooting", *Opt. Laser Technol.*, 111 (2019) 720-726.
[24] N.A. Alnidawi and S.J. Kadhim, "Synthesis and characterizations of core-shell SiO_2/Au/Ag nano-particles by exploding of wire and pulsed laser plasmas", *AIP Conf. Proc.*, 2372(1) (2021) 180004.
[25] S.H. Abdullah, H.R. Humud and F.I. Mustafa, "A Single Layer of Chromium Oxide Nanoparticles Films Coated with Carbon by Applying Exploding Wire Technique for Efficient Solar Selective Absorber", *Iraqi J. Sci.*, 63(10) (2022) 4273-4281.
[26] P. Peerakiatkhajohn et al., "Efficient and rapid photocatalytic degradation of methyl orange dye using Al/ZnO nanoparticles", *Nanomaterials*, 11(4) (2021) 1-13.
[27] E. Chalangar et al., "Influence of morphology on electrical and optical properties of graphene/Al-doped ZnO-nanorod composites", *Nanotechnology*, 29(41) (2018) 415201.
[28] J. Lu et al., "Direct resonant coupling of Al surface plasmon for ultraviolet photoluminescence enhancement of ZnO microrods", *ACS Appl. Mater. Interfaces*, 6(20) (2014) 18301-18305.
[29] S.J. Kadhem, "A Spectroscopic and structural study of FeCoSb alloy", *Iraqi J. Phys.*, 17(41) (2019) 67-74.
[30] H.R. Humud, I.M. Abdulmajeed and S.J. Kadhim, "Copper nanoparticles prepared by pulsed exploding wire", *Iraqi J. Phys.*, 13 (2015) 26.
[31] M.M. Hameed, A.M.E. Al-Samarai and K.A. Aadim, "Synthesis and characterization of gallium oxide nanoparticles using pulsed laser deposition", *Iraqi J. Sci.*, 61(10) (2020) 2582-2589.
[32] L.R. Hou et al., "Interfacial hydrothermal synthesis of SnO_2 nanorods towards photocatalytic degradation of methyl orange", *Mater. Res. Bull.*, 60 (2014) 1-4.
[33] K.A. Aadim and M.M. Shehab, "Influence of Laser Energy on the Structural and Optical Properties of (CdO):(CoO) Thin Films Produced by Laser-Induced Plasma (LIP)", *Iraqi J. Phys.*, 19(49) (2021) 42-52.
[34] S.K. Mustafa, R.K. Jamal and K.A. Aadim, "Studying the effect of annealing on optical and structure properties of ZnO nanostructure prepared by laser induced plasma", *Iraqi J. Sci.*, 60(10) (2019) 2168-2176.
[35] C.V. Reddy et al., "Structural, optical, and improved photocatalytic properties of CdS/SnO_2 hybrid photocatalyst nanostructure", *Mater. Sci. Eng. B*, 221 (2017) 63-72.
[36] M. Vamsi Krishna and M.A. Xavior, "Experiment and statistical analysis of end milling parameters for Al/SiC using response surface methodology", *Int. J. Eng. Technol.*, 7 (2015) 2274-2285.
[37] R.S. Mohammed, K.A. Aadim and K.A. Ahmed, "Estimation of in vivo toxicity of MgO/ZnO core/shell nanoparticles synthesized by eco-friendly non-thermal plasma technology", *Appl. Nanosci.*, 12(12) (2022) 3783-3795.
[38] I.K. Abbas and K.A. Aadim, "Synthesis and Study of Structural Properties of Calcium Oxide Nanoparticles Produced by Laser-Induced Plasma and its Effect on Antibacterial Activity", *Sci. Technol. Indones.*, 7(4) (2022) 427-434.
[39] R.E. Marotti et al., "Bandgap energy tuning of electrochemically grown ZnO thin films by

thickness and electrodeposition potential", *Sol. Ener. Mater. Sol. cells*, 82(1-2) (2004) 85-103.
[40] G. Kaur, A. Mitra and K.L. Yadav, "Pulsed laser deposited Al-doped ZnO thin films for optical applications", *Prog. Nat. Sci. Mater. Int.*, 25(1) (2015) 12-21.
[41] H.P. de Macedo et al., "Characterization of ZnAl2O4 spinel obtained by hydrothermal and microwave assisted combustion method: a comparative study", *Mater. Res.*, 20 (2017) 29-33.
[42] P. Godse et al., "Effect of annealing on structural, morphological, electrical and optical studies of nickel oxide thin films", *J. Surf. Eng. Mater. Adv. Technol.*, 1(2) (2011) 35.
[43] S. Siragam, R.S. Dubey and L. Pappula, "Investigation of V_2O_5-$ZnAl_2O_4$ composite nanoparticles for C-band microstrip patch antenna applications", *Kuwait J. Sci.*, 50(3B) (2023) 1-9.
[44] Z.M. Abbas and Q.A. Abbas, "Aluminum-doped ZnO nano-laminar structures by pulsed laser ablation for gas sensing application", *J. Opt.*, (2023) 1-14, doi: 10.1007/s12596-023-01192-z.
[45] M.J. Akhtar et al., "Aluminum doping tunes band gap energy level as well as oxidative stress-mediated cytotoxicity of ZnO nanoparticles in MCF-7 cells", *Sci. Rep.*, 5 (2015) 13876.
[46] A. Alqudami and S. Annapoorni, "Fluorescence from metallic silver and iron nanoparticles prepared by exploding wire technique", *Plasmonics*, 2(1) (2007) 5-13.
[47] L. Santhosh Kumar et al., "Thermodynamic modeling and characterizations of Al nanoparticles produced by electrical wire explosion process", *J. Mater. Res.*, 32(4) (2017) 897-909.
[48] L. Wu et al., "Characterization and photocatalytic properties of SnO_2–TiO_2 nanocomposites prepared through gaseous detonation method", *Ceram. Int.*, 43(1) (2017) 1517-1521.
[49] L. Wu et al., "Characterization and photocatalytic properties of nano-Fe_2O_3–TiO_2 composites prepared through the gaseous detonation method", *Ceram. Int.*, 43(16) (2017) 14334-14339.
[50] A.A. Lizunova et al., "Plasmon-Enhanced Ultraviolet Luminescence in Colloid Solutions and Nanostructures Based on Aluminum and ZnO Nanoparticles", *Nanomaterials*, 12(22) (2022) 4051.

